crystals

MDPI

Article

The Electrical Resistivity of Liquid Fe-16wt%S-2wt%Si at High Pressures and the Effect of S and Si on the Dynamo in the Ancient Vestan Core

Erin M. Lenhart, Wenjun Yong and Richard A. Secco *

Department of Earth Sciences, University of Western Ontario, London, ON N6A 3K7, Canada; elenhart@uwo.ca (E.M.L.); wyong4@uwo.ca (W.Y.)
* Correspondence: secco@uwo.ca

Abstract: A critical component of predicting thermal convection and dynamo action in the cores of terrestrial planetary bodies is the adiabatic heat flux at the top of the core. Powders of Fe, FeS, and Fe-9wt%Si were mixed to imitate the core of Asteroid 4 Vesta, which studies of HED meteorites indicate is comprised of 13–16wt%S and 1–2wt%Si. In a 1000-ton cubic anvil press, the voltage drop across an Fe-16wt%S-2wt%Si sample of 8–10 mm^3 was measured at 2, 3, 4, and 5 GPa and ~300–2000 K. The resistivity of Fe-16wt%S-2wt%Si is 400 ± 50 μΩ·cm for 2–5 GPa for the complete liquid state. Using the Wiedemann–Franz Law, this gives an electronic thermal conductivity of 11 ± 1.5 W/m/K for 2–4 GPa at complete melting and an adiabatic heat flow of 55 ± 15 MW at the top of an early Fe-16wt%S-2wt%Si Vestan core. The 2 GPa boundary of the miscibility of Fe-16wt%S-2wt%Si is observed. The adiabatic heat flow through an Fe-16wt%S-2wt%Si core of variable size is discussed, as well as the resistivity of liquid Fe alloy at small planetary core conditions as a function of S and Si alloying composition. On the basis of previous studies on binary and ternary alloys of Fe with S and/or Si, we interpolate the separate effects of S and Si on the resistivity (and inversely on thermal conductivity and core adiabatic heat flow).

Keywords: conductivity; liquid iron; high pressure; vesta; planetary cores; dynamos

Citation: Lenhart, E.M.; Yong, W.; Secco, R.A. The Electrical Resistivity of Liquid Fe-16wt%S-2wt%Si at High Pressures and the Effect of S and Si on the Dynamo in the Ancient Vestan Core. *Crystals* **2024**, *14*, 565. https://doi.org/10.3390/cryst14060565

Academic Editors: Joan-Josep Suñol and Khitouni Mohamed

Received: 22 May 2024
Revised: 14 June 2024
Accepted: 17 June 2024
Published: 19 June 2024

1. Introduction

1.1. Background

The movement of electrically conductive fluids inside a planetary core generates and sustains a strong magnetic field. Density deficits in the outer cores of terrestrial planetary bodies imply the strong presence of light elements, with Si and S among the leading candidates for Earth [1] and Mars [2], respectively. The precise composition of the Fe alloy in a given terrestrial planetary body may greatly influence the physical properties and processes of the liquid core, including thermal convection and conduction and the sustenance of a magnetic dynamo. Therefore, heat flux through the outer cores of terrestrial planetary bodies may be modeled and constrained by experiments at representative conditions of temperature, pressure, and composition.

The most effective experimental method of constraining thermal convection in a terrestrial planetary outer core is subtracting the experimentally estimated heat flux due to conduction from the total amount of heat flux from the core into the mantle. The latter part, heat flux across the core–mantle boundary (CMB), may be estimated indirectly using thermal evolution models, petrological evidence, and thermal boundary layer theory, e.g., [3]. Adiabatic heat flux may be constrained if the thermal conductivity and adiabatic thermal gradient are known. According to the Wiedemann–Franz Law, the electronic thermal conductivity may be estimated from electrical resistivity measurements made on a sample at planetary core conditions, which is useful since direct measurements of thermal conductivity are difficult to obtain. Therefore, measurements of the electrical resistivity of

liquid Fe-S-Si alloys at high pressures are a crucial piece in understanding the heat flux and magnetic field generation of terrestrial planetary bodies throughout their histories.

Several lines of reasoning favour Si and S as major light elements in the outer cores of terrestrial planetary bodies. For the case of Si, partitioning experiments [4] showed that at conditions of up to 2873 K and up to 21 GPa, which simulate a terrestrial planetary core forming in a deep magma ocean, 2–11wt%Si is expected in the core, with lower oxygen fugacities favouring more Si arriving in the core. In the case of Earth, the planetary body with by far the best observed seismology, sound velocity experiments on Fe-Si favour at least 2wt%Si [5] and as high as 6wt%Si [1] in the outer core. Additionally, isotopic studies comparing basalts on both the Earth and the Moon to primitive meteorites have indicated Si in the Earth's core [6]. Terrestrial planetary cores expected to contain abundant Si include the cores of Venus [7] and Mercury [8].

Another leading candidate for the light elements in the core of Earth and similar bodies is S. Rama Murthy and Hall [9] first showed evidence for substantial S in Earth's core by demonstrating the depletion of S in bulk silicate Earth relative to primitive meteorites. Since S is siderophilic, S could have partitioned with Fe into the core during differentiation, e.g., [10]. Farther away from the Sun than the Earth's orbit, S likely condensed in greater quantities because of its lower volatility and partitioned in greater quantities with Fe into the cores of terrestrial planetary bodies such as the Galilean moons [11]. Direct evidence includes S in the form of troilite in Fe meteorites [12], and the compositions of IAB meteorites, which are mostly S > 0.4wt% and as high as ~10wt%S [13,14].

The asteroid 4-Vesta is known to possess a differentiated metal core [15,16]. Studies of howardite–eucrite–diogenite (HED) meteorites have indicated that this core contains abundant S and some Si. Several lines of evidence support Vesta as the origin of the HED class of meteorites, including mineralogical comparisons from the Dawn mission [17]. Paleomagnetic studies of the eucrite meteorite Allan Hills A81001 showed an intrinsically generated magnetic dynamo early in the parent body's history [18].

Based on the abundances of siderophiles in HED meteorites relative to chondritic meteorites, the composition of the Vestan core has been estimated to be 13–16wt%S [19]. Toplis et al. [20] also estimated 13wt% or 16wt%S in the core of a Vestan analogue, depending on the chondritic model used. Based on the enrichment of heavy Si isotopes in HED meteorites relative to chondritic meteorites, ref. [21] estimated the Si abundance in the Vestan core as 1–2wt%. Because many previous studies of the Vestan core [22–25] have focused on the case of no light elements, a composition representing the upper bound of light elements in the Vestan core is most useful for the sake of interpolation, given the uncertainty in the true core composition. This includes the possibility of an even lower percentage of Si than the case in this study of 2wt%Si, since meteoritic Si isotope variations are in part attributable to fractionation in the solar nebula instead of entirely to planetary differentiation [26]. For these reasons, Fe alloyed with 16wt%S and 2wt%Si (hereafter referred to as Fe-16S-2Si) was selected for the experiments in this study.

Within Fe alloys, S and Si are immiscible with one another if each light element exceeds a certain proportion of the alloy. This phenomenon has been observed in the quenched liquid structure [27,28] and used to interpolate the limit of miscibility between S and Si in liquid Fe alloys [29]. With increasing pressure, greater percentages of S and Si together can mix with liquid Fe. The immiscibility limit of Fe-16S-2Si in this study is predicted to lie near 6 GPa (Figure 1). Electron microprobe analysis (EMPA) of post-experimental samples will serve to constrain the lowest pressure at which Fe-16S-2Si is miscible in the liquid state.

1.2. Previous Experiments

Experimental measurements of the resistivity of Fe-S-Si alloys have been made at high temperatures and high pressures in previous studies [30–34]. Several studies have been performed on the binary systems Fe-S and Fe-Si. Those with compositions most similar to Fe-16S-2Si include Fe-24wt%S [35] and Fe-5wt%S [36] in terms of S, and Fe-2wt%Si [37] and Fe-4.5wt%Si [38] in terms of Si. Si is observed to increase the resistivity of Fe, although

the peak resistivity is often at a temperature below the solidus, especially for high levels of Si [37]. In the liquid state, the resistivity found for these alloys is generally 100–200 μΩ·cm. The effect of S in these studies is a similar increase in resistivity to that associated with Si. The resistivity found in the liquid state is 150–500 μΩ·cm, with the highest resistivities found for high S. A sudden change in resistivity is commonly found at the partial melt.

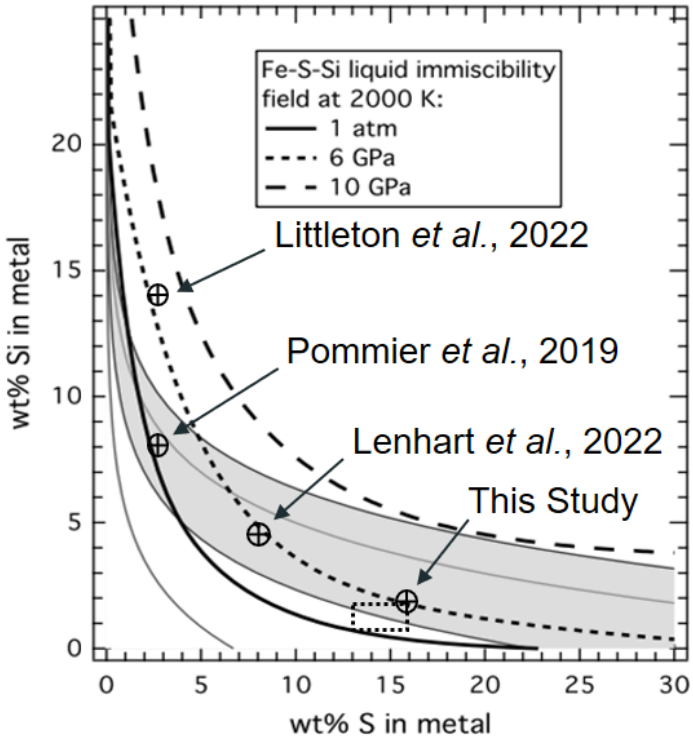

Figure 1. Predicted immiscibility boundaries of Fe-S-Si liquid at 2000 K indicated by dashed lines according to [29]. The compositions of recent studies on Fe-S-Si resistivity at high pressure indicated by circles. Possible compositions of the core of Mercury indicated by the grey region according to [29]. Expected composition of the core of Vesta indicated by a dotted rectangle [19,21]. Citations given in diagram [31–33].

In the ternary system, three experimental resistivity studies at high pressures and high temperatures have been published. These are Pommier et al. [31] with Fe-3wt%S-8wt%Si, Littleton et al. [32] with Fe-3wt%S-14wt%Si, and Lenhart et al. [33] with Fe-8wt%S-4.5wt%Si. Suehiro et al. [34] measured the resistivity of Fe-3wt%S-3wt%Si at high pressures but only at ambient temperature. A quantitative comparison of the effects of total light element percentage on electrical resistivity is provided in the Section 4. These studies show that the effect of increasing the total light element percentage is an increase in estimated electrical resistivity for the liquid state, though not necessarily for the solid state.

To study the effects of Ni on the electrical resistivity of the dominant Fe composition of the core of Vesta, resistivity studies focusing on the effect of Ni ≤ 10wt% on the core of Vesta have been performed [25,39]. These studies indicate that 5–10wt%Ni has a negligible effect on the resistivity of liquid Fe under the conditions of the Vestan core. For this reason, Ni was excluded from the composition used to simulate the core of Vesta in the present study.

2. Materials and Methods

All experiments were performed in a 1000-ton cubic anvil press using the 4-wire method of measuring resistance. The design of the specific pressure cell used is described by Littleton et al. [35]. A labeled cross-section of the sample within the cell is shown in Figure 2 to give context to the images of post-experimental samples in Figures 3 and 4.

Wiring allowed for switching between polarities and between electrodes in type S thermocouple mode.

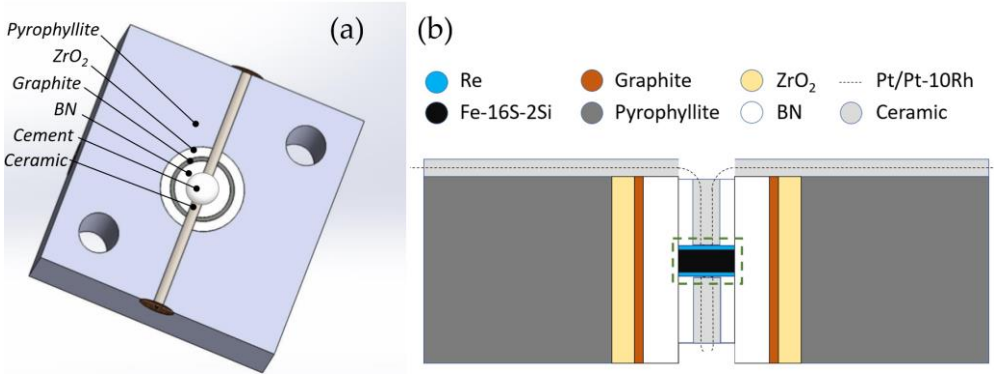

Figure 2. (**a**) The central third of the cubic pressure cell with a side length of 3.18 cm. (**b**) A cross-section of (**a**) with compositions labeled. Cement filled the upper and lower spaces at the bends in the wires. The dotted green box at the center represents the region shown in the compositional maps in Figures 3 and 4.

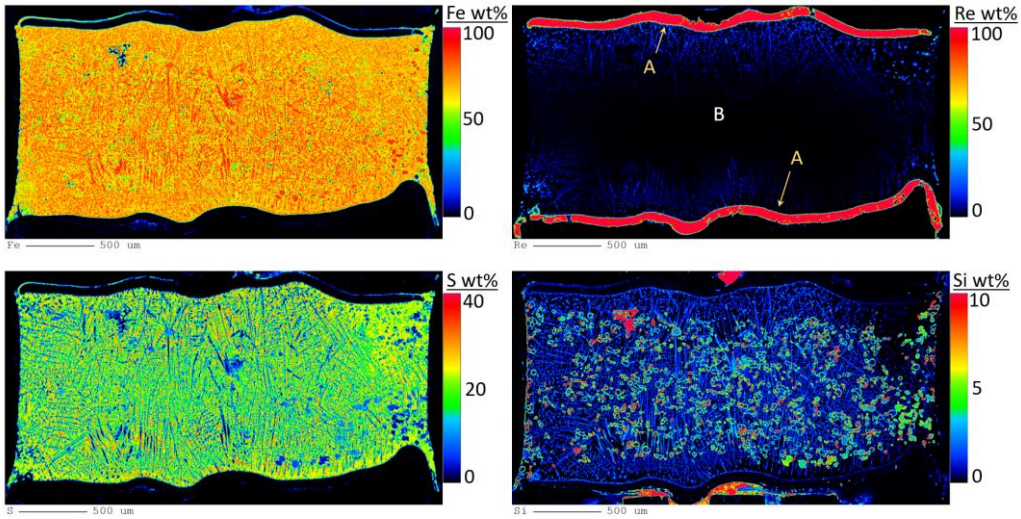

Figure 3. The compositional maps of various elements found by EMPA in a cross-section of a sample recovered from 5 GPa and at ~250 K above the liquidus. The intensity may be taken as an approximation of weight percentage. A indicates the Re disks used to contain the sample. B indicates the Fe-16S-2Si sample itself.

The Fe-16S-2Si sample was mixed from Fe (ESPI Metals, Ashland, OR, USA, 99.95% purity), FeS (Thermo Fisher Scientific, Waltham, MA, USA, 99.98% purity), and Fe-9wt%Si (Goodfellow Cambridge Ltd., Huntingdon, UK, 99.5% purity). The method of weighing and mixing the powders had an associated error of <0.05wt% for each element. EMPA with a $\leq$1.0% error verified the post-experimental Fe-S-Si sample composition. The powder was not previously annealed. In situ at high pressure, the sample was heated to around 973 K for at least five minutes before each experimental run.

During each experimental run, the pressure around the sample was stabilized for a period of an hour or more. Beginning at 298 K, the temperature of the sample was raised by the ohmic heating of a graphite furnace at a rate of approximately 100 K per minute. In situ measurements of the temperature and voltage at each end of the sample were obtained by a four-wire method [25,33,40,41] during the heating process, and measurements were made approximately every 30 s or every 50 K. Samples remained in the liquid state for less than 60 s, during which time measurements were made as often as experimental constraints on

switching polarity allowed. The highest temperatures reached in an experiment varied with pressure from 1950 K to 2050 K. The temperature was then quenched from the maximum temperature.

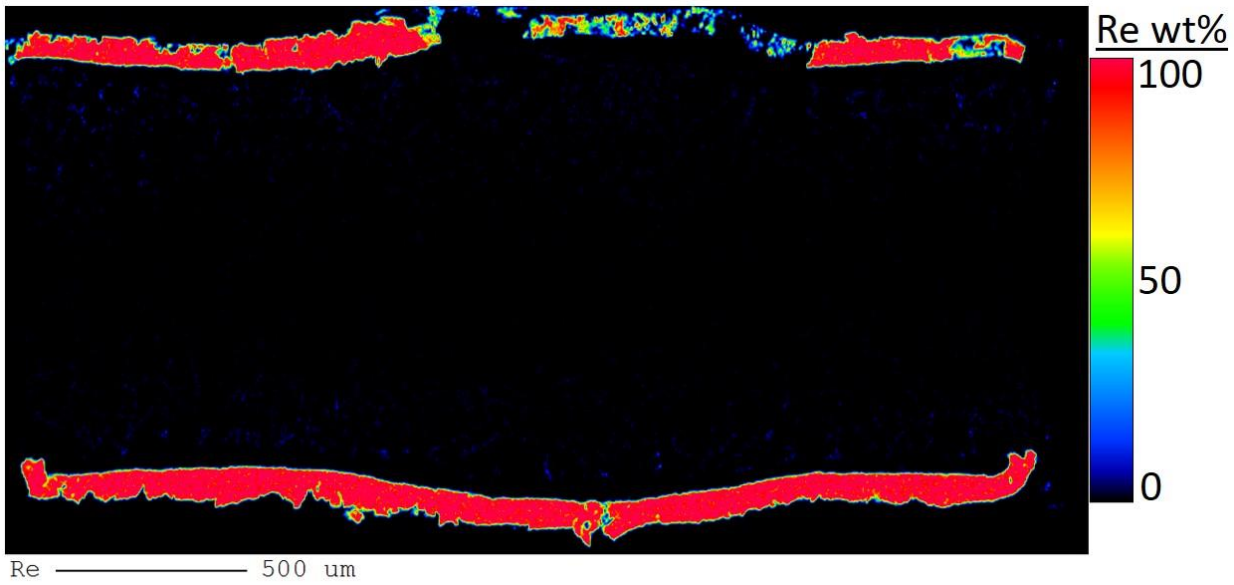

Figure 4. Re in a cross-section of a sample recovered from 5 GPa at a temperature of 1764 K, showing Re does not enter the sample below the liquidus.

To find the electrical resistivity of the material from the voltage drop across the sample, Ohm's and Pouillet's Laws were used. Therefore, in addition to voltage readings, measurements and estimated errors of the constant current and sample geometry were critical. A constant direct current of 0.4 A was generated by a Keysight B2961A power source, which has an error of <1 μA in the relevant current output range. The sample geometry was measured using a Nikon SMZ800 microscope after each experimental run. The measurement tool was accurate to 1 μm, but the uncertainty in the geometry of the sample itself was as high as 100 μm, due largely to variation in the lengths at different locations of each sample.

Several sources of error were considered and combined through standard methods of error propagation (Table 1). Experimental contributions to the error were observed while performing the high-pressure experiments. Because multiple data points were taken for each voltage reading, the standard deviation of these data at each point is a meaningful contribution to error. Such voltage readings include the voltage difference in each thermocouple to find the temperature and the voltage drop across the sample to find resistance using Ohm's Law. Because the resistance was measured in this way, any deviation in the current would also contribute to the error. However, the fluctuations in the current applied from the constant-current power source are negligible (±10 fA) compared to the standard deviation in the voltage.

Table 1. A summary of the sources of error in the resistivity measurements. Actual values vary according to each experiment and according to each data point.

Contribution to Error	Estimated Error Range	Data Units
Voltage Measurement	0.1–2%	mV
Current Variation	10^{-11}–10^{-9}%	A
Sample Geometry Variation	1–10%	mm
Thermocouple Error	0.1–1%	K
Temperature Measurement	0.01–1%	K
Resistivity of Re	0.1–1%	μΩ·cm

The largest source of uncertainty is measurements of sample geometry. Each sample was measured at multiple points along its length and width after grinding. To account for any deviation of the sample shape from a right circular cylinder, an average length was taken, and the variation in length was propagated through Pouillet's Law. The S-type thermocouples used in the experiment had a smaller error associated with the manufacturing of the exact composition, the application of the Seebeck effect to generate an EMF vs. T relation, and the effect of pressure on the EMF. A contribution error of 0.1% is expected. The contribution of the Re disks to the resistivity [41] was accounted for. Additionally, because the electrical resistivity of Re [41] is lower than that of the sample composition, the small amounts (<1wt%; see Figure 4) of Re mixed with the sample upon melting will add a small uncertainty in the resistivity of the sample. However, the loss of Re mass from the disks, leading to a decreased contribution to the overall voltage drop, may be counterbalanced by the addition of Re to the sample, leading to an increased contribution to the overall voltage drop caused by disorder resistivity.

Thermal conductivity was estimated from electrical resistivity and temperature using the Wiedemann–Franz Law: $\kappa_e = LT/\rho$. The Sommerfeld value, $L_0 = 2.44 \times 10^{-8}$ W·Ω/K^2 in SI units, was used and may be taken as a minimum in the pressure, temperature [42], and compositional ranges of this study. Finally, first-principle calculations were performed to estimate the electrical resistivity, thermal conductivity, and Lorenz number (0.94 L_0) of Fe-16S-2Si at these conditions [43]. These density functional theory calculations were performed following similar techniques used in previous papers [44–48]. This is in line with the prediction that Fe may have a Lorenz number lower than the Sommerfeld value at high pressures [49].

Electron Microprobe Analysis

A JXA-8530F electron microprobe (JEOL, Tokyo, Japan) was used to analyze the elemental composition of a variety of samples. Compositional maps were generated for each element across each sample. These were derived from wavelength dispersive spectroscopy (WDS) data for Fe, S, Si, and Re and energy dispersive spectroscopy (EDS) data for Pt and Rh. The standard used was the element itself, except in the case of S, for which pyrite was used. For spot measurements, a beam size of 2 or 5 µm was used, along with a probe current of 60 nA and an accelerating voltage of 15 kV.

The measurement of elemental composition via EMPA offers several insights into sample composition during the experiment. First, it allows the overall composition of each sample to be verified. Second, the scale at which Fe, S, and Si were mixed in the solid state may be deduced, with implications for both homogeneity and miscibility. Third, any contamination by the disk or thermocouples at or before the quenching temperature may be observed. Then, once samples recovered from varying temperatures are probed, the temperature range in which such contamination could begin may be deduced, along with the maximum temperature at which no such contamination occurs.

3. Results

Compositional maps indicating the weight percentages of Fe, S, Si, and Re for a sample are shown in Figure 3.

At the scale of tens of microns, the Fe, S, and Si in the sample are well mixed, with the exception of only a few outlier patches. Even though the melting temperature of Re is more than 1000 K higher than any temperatures reached in these experiments [50], Re from the disk entered the sample in small amounts, accounting for <1wt% of the average composition of the post-experimental sample as averaged point-by-point. Probe images of samples quenched below the melt indicate that most of this Re contamination occurred after the complete melting of the sample, as shown in Figure 4.

To constrain the pressure boundary of the miscibility of Fe-16S-2Si, EMPA results were compared for samples recovered from various pressures. In this recovered sample, EMPA results show that Fe-16S-2Si is miscible on the scale of tens of microns at pressures as low

as 3 GPa. At only 2 GPa, however, Figure 5 shows that S and Si separate into immiscible regions within the quenched liquid Fe alloy.

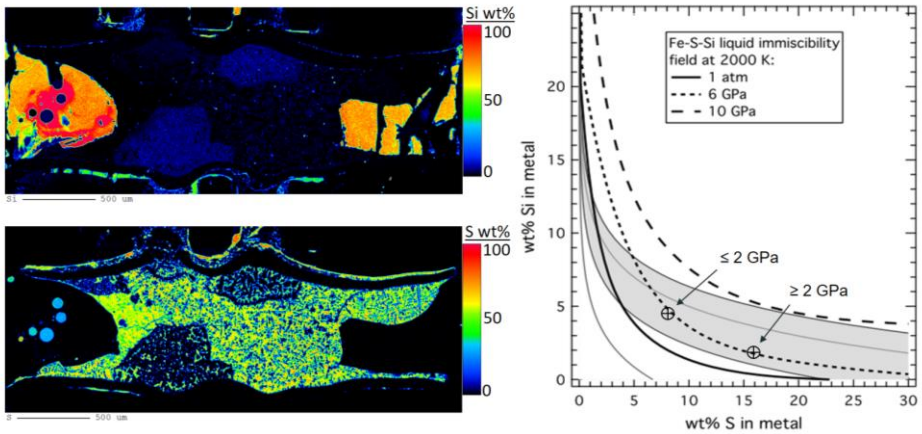

Figure 5. S and Si found by EMPA for an Fe-16S-2Si sample recovered from 2 GPa and above the liquidus. Note the regions of high Si and negligible S on each end, which contain spherules of Fe-S on the scale of 0.1 mm. Experimental constraints on the pressure boundary of the immiscibility of Fe-S-Si from this study on Fe-16S-2Si and Lenhart et al. [33] on Fe-4.5S-8Si are added to the plot according to Chabot et al. [29] shown in Figure 1.

The electrical resistivity results of Fe-16S-2Si found using Ohm's and Pouillet's Laws are displayed in Figure 6. The eutectic melting in Fe-S begins at ~1250 K and ends at ~1450 K [51], with the eutectic temperature constant up to at least 8 GPa [52]. A flattening in resistivity is seen above the liquidus, especially for the data at 4 GPa and 5 GPa. The data at 2 GPa may show unexpected trends due to the immiscibility of small amounts of Fe-Si in the larger Fe-S matrix (see Figure 5).

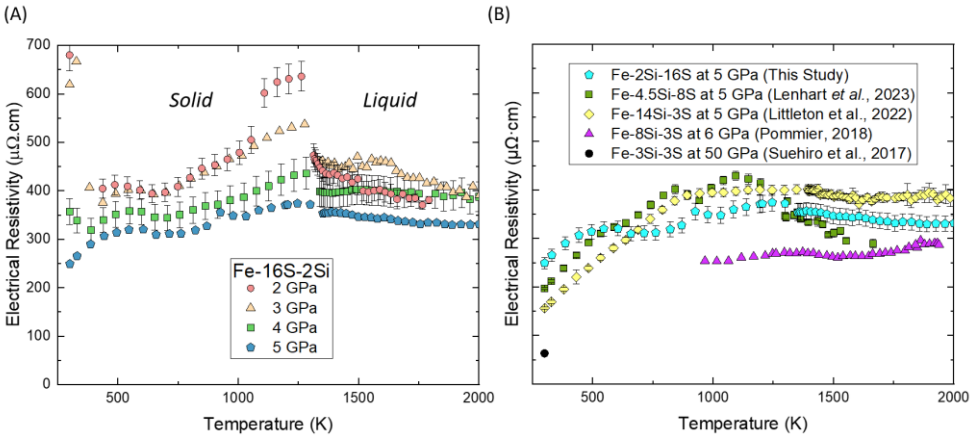

Figure 6. (**A**) Electrical resistivity of Fe-16S-2Si measured from 2–5 GPa and into the liquid state. Estimated errors are given for the 4 GPa data. (**B**) Electrical resistivity of various Fe-S-Si compositions measured near 5 GPa and into the liquid state. Citations given in plot [31–34].

Previous studies of Fe-S-Si resistivity are plotted with the results of this study in Figure 6b in order to show the differing effects of S and Si on the resistivity of Fe. As expected, both alloying S and alloying Si increase the resistivity of Fe. In the liquid state, Si tends to have a larger increase in resistivity per increase in weight percentage, as observed in the difference between Fe-16S-2Si and Fe-3S-14Si. This is the opposite trend compared to much of the solid state. This trend reduces slightly when stated in terms of atomic percentage. Si still may have a larger effect on resistivity than S in such a case.

Finally, from first-principle calculations, M. Pozzo [43] has estimated the phononic contribution to the electrical resistivity of Fe-16S-2Si to be 129 μΩ·cm at 5 GPa and 1979 K. If we treat this as accounting for 40% of the total resistivity (60% of the total resistivity has a magnetic origin; [53]) measured in our study, then a total calculated resistivity would be 323 μΩ·cm. This agrees well with the experimental result of 340 ± 25 μΩ·cm shown in Figure 6a.

The thermal conductivity results found using the Wiedemann–Franz Law and the Sommerfeld value of the Lorenz number are displayed in Figure 7.

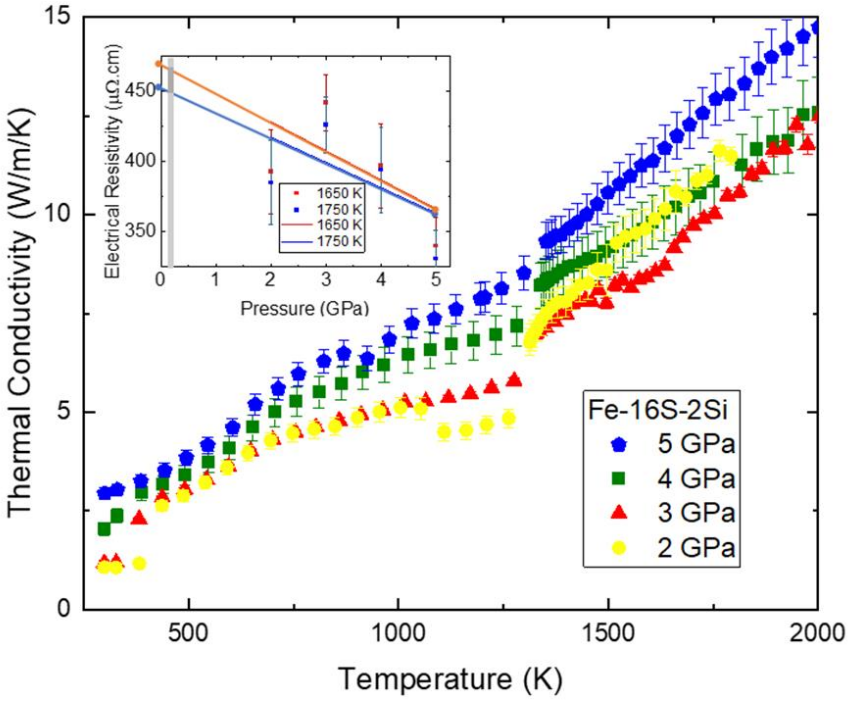

Figure 7. Thermal conductivity of Fe-16S-2Si calculated using the Sommerfeld value of the Lorenz number measured from 2 to 5 GPa and into the liquid state with representative error bars shown on the 4 GPa data set. The resistivity with pressure is shown near the liquidus (inset) and used to extrapolate to the pressure of the core of Vesta (shown in grey).

The thermal conductivity of Fe-16S-2Si in the pressure range of interest increases roughly linearly with temperature. A sudden increase occurs at the start of Fe-S eutectic melting around 1250 K. The data generally show increasing thermal conductivity with increasing pressure at constant temperature, although in the liquid state, the thermal conductivity data overlaps within the boundaries of estimated error in the case of 2–4 GPa.

The effect of pressure on resistivity near the complete melt is shown in the inset of Figure 7. As expected, increasing pressure results in a decrease in resistivity. This effect exceeds the estimated error of the study. Still, across this study, pressure increases by a factor of 2.5 while resistivity only decreases by a factor of 0.8–0.9.

4. Discussion

The electrical resistivity of Fe-16S-2Si from this study is compared to previously measured values near 5 GPa and the melt of pure Fe (~1800 K) in Figure 8.

S (wt%)	Si (wt%)	$Q_{5GPa,1800K}$ (μΩ·cm)	Reference
0	0	115	Silber et al., 2018
0	4.5	120	Silber et al., 2019
0	8.5	150	Berrada et al., 2020
5	0	220*	Pommier, 2018
3	8	290*	Pommier et al., 2019
3	14	370	Littleton et al., 2022
8	4.5	259	Lenhart et al., 2023
16	2	341	This Study

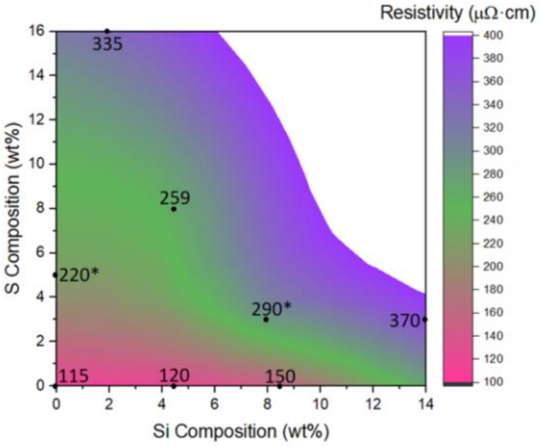

Figure 8. The measured electrical resistivity values (black points) of Fe(-S)(-Si) alloys at 5 GPa and 1800 K interpolated as a resistivity map. * Pressure difference of 0.5–1 GPa. Citations given in table [31–34,36–38,54].

As expected, the resistivity tends to increase with increasing S and with increasing Si because Fe is more conductive than each light element is. The rate of this increase in resistivity with each light element is visualized in Figure 8. Comparing and interpolating the electrical resistivity values of Fe-S-Si alloys allows for a more general discussion of terrestrial planetary bodies with S and Si as the predominant light alloying elements in the liquid core. Such interpolations have value for the discussion of heat flux and magnetic field generation in the cores of such bodies. For example, the ranges of pressure and S content may be particularly relevant to the cores of the Galilean moons, such as Ganymede.

4.1. Heat Flux in the Core of Early Vesta

To estimate the heat flux in the core of early Vesta, estimates of the thermal conductivity in the core are needed; these, in turn, depend on the composition of the core (see Figure 8). As stated in the Introduction, the S and Si amounts in the composition of this study are within the expected bounds of the Vestan core composition. However, this composition is one end of a range of plausible compositions for the Vestan core, deliberately selected on the high end of the expected light element proportion in order to supplement previous resistivity studies and Vestan core studies alike, which focus on the case of no light elements.

Extrapolating to the pressure of the outermost core of Vesta, 0.1–0.2 GPa [25], and the temperature of crystallization gives a thermal conductivity value of 9.5 ± 1.5 W/m/K, considering measured values of resistivity for Fe-16S-2Si. While the composition of this study may lead to immiscible Fe-S and Fe-Si layers based on the limited Fe-S-Si miscibility information available in the literature, a small reduction in either S or Si would likely be miscible at the pressures of the core of Vesta. The largest reduction in light elements still within the predicted range [19,21] could correspond to a thermal conductivity as high as 12 W/m/K, considering errors in measurement and in actual core composition.

While speculative, the results of this study may additionally be used to discuss the case of a Vestan core with two immiscible layers: Fe-S and Fe-Si. On the basis of limited EMP analyses of the 2 GPa recovered sample (Figure 5), the Fe-S liquid may contain ~26wt%S. This would leave the Fe-Si liquid with ~5.2wt%Si. Figure 8 estimates the electrical resistivity of such binary compositions, but not for such high S compositions as 26wt%. However, a previous study [35] provides resistivity values for this composition. The high Fe-26wt%S resistivity implies a low thermal conductivity, but the low Fe-5.2wt%Si resistivity implies a high thermal conductivity. The physical distribution of these phases in a Vestan core would need to be modeled in order to determine the resulting effect of liquid immiscibility on net thermal conductivity.

With thermal conductivity values for the miscible Fe-S-Si case, the adiabatic heat flux through the top of a core of the given composition, q, may be estimated by Fourier's Law,

$$q = -\kappa \nabla T, \quad (1)$$

for thermal conductivity, κ, and adiabatic thermal gradient, ∇T. The adiabatic thermal gradient can, in turn, be derived from Maxwell's relations as $\nabla T = (\partial T/\partial r)_S = (\partial T/\partial P)_S \partial P/\partial r = \alpha g T/C_P$ for thermal expansivity, α; gravitational acceleration, g; temperature, T; and heat capacity at constant pressure, C_P.

Values for α, g, T, and C_P are needed to estimate the adiabatic heat flux. These may depend on conditions of pressure, which, in the case of a given planetary body, may be estimated from equations of hydrostatic equilibrium. The thermal expansivity for Fe-16S-2Si may be estimated from studies on Fe-16wt%S [55] as 8×10^{-5} K^{-1}, with the effect of 2wt%Si taken to be negligible [56]. Gravitational acceleration at the top of the core of Vesta can be calculated as 0.2 m/s^2 in the case of an Fe-16wt%S with a density of 5200 kg/m^3 [57]. The heat capacity of Fe alloys may be taken as ~800 J/K/kg (e.g., [23]). This gives an adiabatic heat flux at the top of the core of 0.3–0.4 mW/m^2 and a corresponding adiabatic heat flow of 55 ± 15 MW. Considering the lowest estimates of S and Si in the Vestan core [19–21], this number could be as high as 80 MW.

Compared to previous estimates of adiabatic heat flow at the top of the core of early Vesta [25,39], this result is much lower or at the low end of a broad range [24] due to the effects of the light elements likely to be present. The consideration of these light elements greatly lowers the predicted thermal conductivity of the core and additionally lowers the estimated gravitational acceleration at the top of the core, thereby lowering the adiabatic thermal gradient. This demonstrates that light elements should not be omitted from future models of heat flow in the Vestan core. The estimate of 55 ± 15 MW for the adiabatic heat flux at the top of the core of Vesta with Fe-16S-2Si is much smaller than that of other similar planetary bodies that have been studied, such as the Moon or Ganymede [35,36,58]. This difference is due partly to the consideration of light elements but mainly to the differences in core sizes.

To find the convective heat flux, F_{Conv}, the maximum amount of heat flux that conduction is capable of may be subtracted from the total amount of heat flux from the Vestan core into the mantle. Previous models have estimated such a total heat flux through the core–mantle boundary. Weiss et al. [23] used $F_{Total} = \rho_C r_C C_P/3 \times dT/dt$ to estimate 500 mW/m^2 as the heat flux from the top of the Fe core of Vesta into its mantle. Formisano et al. [24] estimated only 10 mW/m^2 as the peak heat flux. In either case, the adiabatic heat flux found in Equation (1) is 2–3 orders of magnitude lower than these values, giving >10 mW/m^2 as F_{Conv} in the early Vestan core. The vigor of thermal convection would, of course, be mitigated by any contribution from compositional convection, but the importance or even existence of compositional convection cannot be known until the presence of a solid inner core in Vesta is proven.

The presence of thermal convection in Fe alloys does not lead to dynamo action in all cases. As a basic indicator of whether dynamo action would occur in the core of Vesta, the magnetic Reynolds number, Re_m, may be used. Using Re_m, the characteristic velocity, U, may be calculated by $U = Re_m \times \rho/\mu/L$, for magnetic permeability, $\mu = 4\pi \times 10^{-7}$ H/m, and core length, L = 110 ± 3 km [15] in the case of Vesta. For a threshold Re_m of π^2 and a resistivity of 450 ± 40 μΩ·cm found in this study, a value of $U > 0.35$ mm/s is needed for magnetic dynamo formation. For context, the characteristic velocity of the Fe alloys in the outer core of the Earth is estimated as 0.07–0.7 mm/s [59]. This threshold value found for Fe-16S-2Si is more than double the threshold value in the case of Fe-Ni [25]. Since the effect of these light elements on the convective heat flux discussed above is not as strong, the overall effect of light elements is likely a reduction in the expected duration of the dynamo as Vesta cools due primarily to their effect on the threshold of the magnetic Reynold's number.

Based on the estimated convective heat flux, the characteristic velocity generated by thermal convection in Vesta may be estimated. For example, ref. [60] estimated the characteristic velocity with $U = (F_{Conv} g \alpha l / 3.3 / \rho^* / C_P)^{1/3}$. Estimates for all these values may be found above. Density, ρ^*, was estimated as $\rho^* = 5200$ kg/m^3, accounting for the pressure and sulfur content of the sample [61] in the Birch–Murnaghan equation of state [57]. This gives $U = 0.1$–0.4 mm/s, with the lower end of that range more likely. This range is in very good agreement with the estimate found using the magnetic Reynolds number above.

Previous studies of the early Vestan dynamo have often assumed a core composition of pure Fe. For the cases of other compositions, previous studies have demonstrated a near-negligible effect of $\leq$10wt%Ni in the core of Vesta [25,39]. The current study predicts the effect of light elements S and Si on the adiabatic heat flux through the early Vestan core. In particular, the value of 0.3–0.4 mW/m^2 found in Equation (1) is much less than any estimate of the total heat flux from the core into the mantle of early Vesta, and less than half of that predicted for the case of pure Fe. The adiabatic heat flux is much less than the total heat flux out of the core of Vesta before solidification, as estimated by Weiss et al. [23]. Therefore, accounting for these alloying elements raises the estimated convective heat flux as a function of time due to the alloyed composition's lower thermal conductivity and associated adiabatic heat flux.

4.2. Modeling Heat Flow by Fe-16S-2Si Core Size

Using the results of this and other studies [23,55,56], the adiabatic heat flow at the top of the core of a small terrestrial planetary body with an Fe-S-Si core may be estimated as shown in Figure 9. For this study, a core of Fe-16S-2Si was assumed, but any Fe-S-Si core within the miscibility limit of S and Si could be constrained with the use of other resistivity studies of liquid Fe-S-Si alloys at similar pressures [31–33].

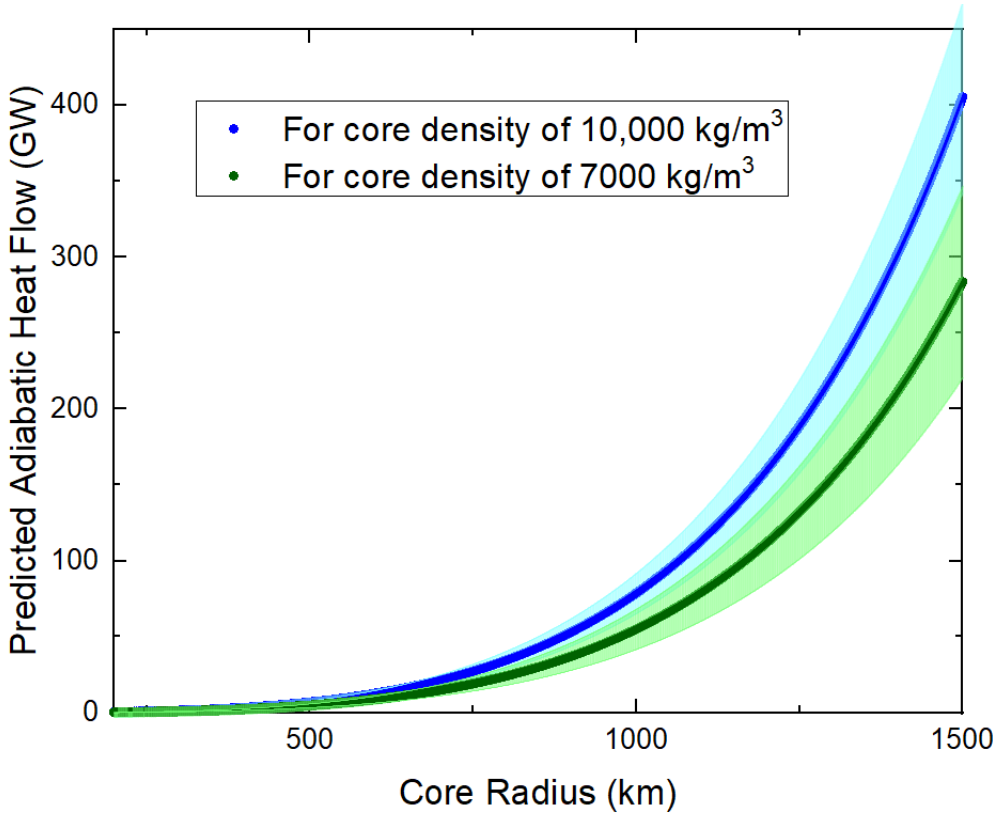

Figure 9. The predicted adiabatic heat flow through the top of a sub-Earth planet with an Fe-16S-2Si core. Error is estimated in the shaded areas.

Besides thermal conductivity, the physical properties of Fe-S-Si used to calculate the adiabatic temperature gradient were considered in finding the results in Figure 9. In particular, thermal expansivity, α, varies with temperature and composition. Given that α of Fe-4.7wt%Si has been experimentally measured as almost identical to that of pure Fe [56], 2wt%Si is unlikely to significantly affect the thermal expansivity of Fe-16wt%S. To constrain the effect of S on α of Fe as a function of temperature and pressure, measurements by Chen et al. [55] were used. The largest contributions to the uncertainties reflected in the shaded area of Figure 9 are the uncertainties in the coefficient of thermal expansion and the experimental uncertainties in determining the thermal conductivity detailed above.

5. Conclusions

The electrical resistivity of Fe-16S-2Si has been measured in the liquid state at 2-5 GPa. The thermal conductivity at the top of a liquid Fe-16S-2Si core was found according to the Wiedemann-Franz Law. The adiabatic heat flow at the top of small terrestrial planetary cores was calculated and has important implications for predicting thermal convection and dynamo action. For Asteroid 4 Vesta with a liquid Fe-16S-2Si core, the adiabatic heat flow at the top of the core is estimated to be 55 ± 15 MW—less than half of what would be predicted for the case of pure Fe. Future studies could add more data to Figure 8 to better constrain the thermal conductivity of Fe-S-Si alloys in small planetary bodies, which will lead to better estimates of adiabatic heat flow in cores with different Fe-S-Si compositions.

Author Contributions: Conceptualization, R.A.S.; methodology, E.M.L. and W.Y.; validation, W.Y. and R.A.S.; formal analysis, E.M.L.; investigation, E.M.L. and W.Y.; resources, R.A.S. and W.Y.; data curation, E.M.L.; writing—original draft preparation, E.M.L.; writing—review and editing, W.Y. and R.A.S.; supervision, W.Y. and R.A.S.; project administration, R.A.S. and W.Y.; funding acquisition, R.A.S. and W.Y. All authors have read and agreed to the published version of the manuscript.

Funding: This work was supported by the Natural Sciences and Engineering Research Council of Canada to R.A.S. [RGPIN-2018-05021] and to W.Y. [RGPIN-2022-04427, DGECR-2022-00151]. E.M.L. gratefully acknowledges funding for graduate study through a Queen Elizabeth II Scholarship.

Data Availability Statement: The original contributions presented in the study are included in the article, further inquiries can be directed to the corresponding author.

Acknowledgments: We thank those who contributed to these experiments. Jonathan Jacobs helped in machining many of the parts for the pressure cells. Stephen Wood prepared the post-experimental samples for EMPA. Joshua Laughton performed the EMPA, including creating detailed compositional maps of the samples.

Conflicts of Interest: The authors declare no conflicts of interest.

References

1. Zhang, Y.; Sekine, T.; He, H.; Yu, Y.; Liu, F.; Zhang, M. Experimental constraints on light elements in the Earth's outer core. *Sci. Rep.* **2016**, *6*, 22473. [CrossRef]
2. Khan, A.; Sossi, P.A.; Liebske, C.; Rivoldini, A.; Giardini, D. Geophysical and cosmochemical evidence for a volatile-rich Mars. *Earth Planet. Sci. Lett.* **2022**, *578*, 117330. [CrossRef]
3. Frost, D.A.; Avery, M.S.; Buffett, B.A.; Chidester, B.A.; Deng, J.; Dorfman, S.M.; Li, Z.; Liu, L.; Lv, M.; Martin, J.F. Multidisciplinary Constraints on the Thermal-Chemical Boundary Between Earth's Core and Mantle. *Geochem. Geophys. Geosystems* **2022**, *23*, e2021GC009764. [CrossRef]
4. Ricolleau, A.; Fei, Y.W.; Corgne, A.; Siebert, J.; Badro, J. Constraints on oxygen and silicon contents of Earth's core from metal-silicate partitioning experiments at high pressure and temperature. *Earth Planet. Sci. Lett.* **2011**, *310*, 409–421. [CrossRef]
5. Badro, J.; Fiquet, G.; Guyot, F.; Gregoryanz, E.; Occelli, F.; Antonangeli, D.; d'Astuto, M. Effect of light elements on the sound velocities in solid iron: Implications for the composition of Earth's core. *Earth Planet. Sci. Lett.* **2007**, *254*, 233–238. [CrossRef]
6. Georg, R.B.; Halliday, A.N.; Schauble, E.A.; Reynolds, B.C. Silicon in the Earth's core. *Nature* **2007**, *447*, 1102–1106. [CrossRef]
7. Trønnes, R.G.; Baron, M.A.; Eigenmann, K.R.; Guren, M.G.; Heyn, B.H.; Løken, A.; Mohn, C.E. Core formation, mantle differentiation and core-mantle interaction within Earth and the terrestrial planets. *Tectonophysics* **2019**, *760*, 165–198. [CrossRef]
8. Malavergne, V.; Toplis, M.J.; Berthet, S.; Jones, J. Highly reducing conditions during core formation on Mercury: Implications for internal structure and the origin of a magnetic field. *Icarus* **2010**, *206*, 199–209. [CrossRef]

9. Rama Murthy, V.; Hall, H.T. The Chemical Composition of the Earth's Core: Possibility of Sulfur in the Core. *Phys. Earth Planet. Inter.* **1970**, *2*, 276–282. [CrossRef]
10. Chabot, N.L.; McDonough, W.F.; Jones, J.H.; Saslow, S.A.; Ash, R.D.; Draper, D.S.; Agee, C.B. Partitioning behavior at 9 GPa in the Fe–S system and implications for planetary evolution. *Earth Planet. Sci. Lett.* **2009**, *305*, 425–434. [CrossRef]
11. Keszthelyi, L.; Jaeger, W.L.; Turtle, E.P.; Milazzo, M.; Radebaugh, J. A post-Galileo view of Io's interior. *Icarus* **2004**, *169*, 271–286. [CrossRef]
12. Von Reichenbach, K.L. Über das innere Gefüge der näheren Bestandtheile des Meteoreisens. *Ann. Der Phys. Chem.* **1861**, *21*, 99–132. [CrossRef]
13. Buchwald, V.F. *Handbook of Iron Meteorites*; University California Press: Oakland, CA, USA, 1975; 1418p.
14. Wasson, J.T.; Kallemeyn, G.W. The IAB iron-meteorite complex: A group, five subgroups, numerous grouplets, closely related, mainly formed by crystal segregation in rapidly cooling melts. *Geochim. Cosmochim. Acta* **2002**, *66*, 2445–2473. [CrossRef]
15. Russell, C.T.; Raymond, C.A.; Coradini, A.; Mcsween, H.Y.; Zuber, M.T.; Nathues, A.; Sanctis, M.C.D.E.; Jaumann, R.; Konopliv, A.S.; Preusker, F.; et al. Dawn at Vesta: Testing the Protoplanetary Paradigm. *Science* **2012**, *336*, 684–686. [CrossRef]
16. Ermakov, A.I.; Zuber, M.T.; Smith, D.E.; Raymond, C.A.; Balmino, G.; Fu, R.R.; Ivanov, B.A. Constraints on Vesta's interior structure using gravity and shape models from the Dawn mission. *Icarus* **2014**, *240*, 146–160. [CrossRef]
17. Mittlefehldt, D.W. Asteroid (4) Vesta: I. The howardite-eucrite-diogenite (HED) clan of meteorites. *Chem. Erde* **2015**, *75*, 155–183. [CrossRef]
18. Fu, R.R.; Weiss, B.P.; Shuster, D.L.; Gattacceca, J.; Grove, T.L.; Suavet, C.; Lima, E.A.; Li, L.; Kuan, A.T. An ancient core dynamo in asteroid Vesta. *Science* **2012**, *338*, 238–241. [CrossRef]
19. Steenstra, E.S.; Dankers, D.; Berndt, J.; Klemme, S.; Matveev, S.; van Westrenen, W. Significant depletion of volatile elements in the mantle of asteroid Vesta due to core formation. *Icarus* **2019**, *317*, 669–681. [CrossRef]
20. Toplis, M.J.; Mizzon, H.; Monnereau, M.; Forni, O.; McSween, H.Y.; Mittlefehldt, D.W.; McCoy, T.J.; Prettyman, T.H.; De Sanctis, M.C.; Raymond, C.A.; et al. Chondritic models of 4 Vesta: Implications for geochemical and geophysical properties. *Meteorit. Planet. Sci.* **2013**, *48*, 2300–2315. [CrossRef]
21. Pringle, E.A.; Savage, P.S.; Badro, J.; Barrat, J.-A.; Moynier, F. Redox state during core formation on asteroid 4-Vesta. *Earth Planet. Sci. Lett.* **2013**, *373*, 75–82. [CrossRef]
22. Dreibus, G.; Bruckner, J.; Wanke, H. On the Core Mass of the Asteroid Vesta. *Meteorit. Planet. Sci.* **1997**, *32*, A36.
23. Weiss, B.P.; Gattacceca, J.; Stanley, S.; Rochette, P.; Christensen, U.R. Paleomagnetic Records of Meteorites and Early Planetesimal Differentiation. *Space Sci. Rev.* **2010**, *152*, 341–390. [CrossRef]
24. Formisano, M.; Federico, C.; De Angelis, S.; De Sanctis, M.C.; Magni, G. A core dynamo in Vesta? *Mon. Not. R. Astron. Soc.* **2016**, *458*, 695–707. [CrossRef]
25. Lenhart, E.M.; Secco, R.A. Implications for the Energy Source for an Early Dynamo in Vesta from Experiments on Electrical Resistivity of Liquid Fe-10wt%Ni at High Pressures. *Icarus* **2022**, *378*, 114962. [CrossRef]
26. Dauphas, N.; Poitrasson, F.; Burkhardt, C.; Kobayashi, H.; Kurosawa, K. Planetary and meteoritic Mg/Si and δ30Si variations inherited from solar nebula chemistry. *Earth Planet. Sci. Lett.* **2015**, *427*, 236–248. [CrossRef]
27. Sanloup, C.; Fei, Y. Closure of the Fe–S–Si liquid miscibility gap at high pressure. *Phys. Earth Planet. Inter.* **2004**, *147*, 57–65. [CrossRef]
28. Morard, G.; Katsura, T. Pressure-temperature cartography of Fe-S-Si immiscibility system. *Geochim. Cosmochim. Acta* **2010**, *74*, 3659–3667. [CrossRef]
29. Chabot, N.L.; Wollack, E.A.; Klima, R.L.; Manitti, M.E. Experimental constraints on Mercury's core composition. *Earth Planet. Sci. Lett.* **2014**, *390*, 199–208. [CrossRef]
30. Berrada, M.; Secco, R.A. Review of Electrical Resistivity Measurements and Calculations of Fe and Fe-Alloys Relating to Planetary Cores. *Front. Earth Sci.* **2021**, *9*, 732289. [CrossRef]
31. Pommier, A.; Leinenweber, K.; Tran, T. Mercury's thermal evolution controlled by an insulating liquid outermost core? *Earth Planet. Sci. Lett.* **2019**, *517*, 125–134. [CrossRef]
32. Littleton, J.A.H.; Yong, W.; Secco, R.A. Electrical resistivity of the Fe-Si-S ternary system: Implications for timing of thermal convection shutdown in the lunar core. *Sci. Rep.* **2022**, *12*, 19031. [CrossRef]
33. Lenhart, E.M.; Yong, W.; Secco, R.A.; Flemming, R. Electrical resistivity of liquid Fe-8wt%S-4.5wt%Si at high pressures with implications for heat flux through the cores of Io and sub-earth exoplanets. *Icarus* **2023**, *395*, 115472. [CrossRef]
34. Suehiro, S.; Ohta, K.; Hirose, K.; Morard, G.; Ohishi, Y. The influence of sulfur on the electrical resistivity of hcp iron: Implications for the core conductivity of Mars and Earth. *Geophys. Res. Lett.* **2017**, *44*, 8254–8259. [CrossRef]
35. Littleton, J.A.H.; Secco, R.A.; Yong, W. Thermal Convection in the Core of Ganymede Inferred from Liquid Eutectic Fe-FeS Electrical Resistivity at High Pressures. *Crystals* **2021**, *11*, 875. [CrossRef]
36. Pommier, A. Influence of sulfur on the electrical resistivity of a crystallizing core in small terrestrial bodies. *Earth Planet. Sci. Lett.* **2018**, *496*, 37–46. [CrossRef]
37. Berrada, M.; Secco, R.A.; Yong, W.; Littleton, J.A.H. Electrical Resistivity Measurements of Fe-Si with Implications for the Earth Lunar Dynamo. *J. Geophys. Res.* **2020**, *125*, e2020JE006380. [CrossRef]
38. Silber, R.E.; Secco, R.A.; Yong, W.; Littleton, J.A.H. Heat Flow in Earth's Core from Invariant Electrical Resistivity of Fe-Si on the Melting Boundary to 9 GPa: Do Light Elements Matter? *J. Geophys. Res.* **2019**, *124*, 5521–5543. [CrossRef]

39. Orole, O.A.; Wenjun, Y.; Secco, R.A. Thermal Convection in Vesta's Core from Experimentally-Based Conductive Heat Flow Estimates. *Crystals* **2022**, *12*, 1752. [CrossRef]
40. Ezenwa, I.C.; Secco, R.A. Electronic transition in solid Nb at high pressure and temperature. *J. Appl. Phys.* **2017**, *121*, 22. [CrossRef]
41. Littleton, J.A.H.; Secco, R.A.; Yong, W.; Berrada, M. Electrical resistivity and thermal conductivity of W and Re up to 5 GPa and 2300 K. *J. Appl. Phys.* **2019**, *125*, 13. [CrossRef]
42. Zhang, Y.; Luo, K.; Hou, M.; Driscoll, P.; Salke, N.P.; Minár, J.; Prakapenka, V.B.; Greenberg, E.; Hemley, R.J.; Cohen, R.E.; et al. Thermal conductivity of Fe-Si alloys and thermal stratification in Earth's core. *Proc. Natl. Acad. Sci. USA* **2021**, *119*, e2119001119. [CrossRef]
43. Pozzo, M. (Department of Earth Sciences, University College London, London, UK). Personal communication, 2023.
44. Pozzo, M.; Davies, C.; Gubbins, D.; Alfè, D. Thermal and electrical conductivity of iron at Earth's core conditions. *Nature* **2012**, *485*, 355–358. [CrossRef]
45. Pozzo, M.; Davies, C.; Gubbins, D.; Alfè, D. Transport properties for liquid silicon-oxygen-iron mixtures at Earth's core conditions. *Phys. Rev. B* **2013**, *87*, 014110. [CrossRef]
46. Pozzo, M.; Davies, C.; Gubbins, D.; Alfè, D. Thermal and electrical conductivity of solid iron and iron–silicon mixtures at Earth's core conditions. *Earth Planet. Sci. Lett.* **2014**, *393*, 159–164. [CrossRef]
47. Pozzo, M.; Alfè, D. Saturation of electrical resistivity of solid iron at Earth's core conditions. *SpringerPlus* **2016**, *5*, 256. [CrossRef]
48. Pozzo, M.; Davies, C.J.; Alfè, D. Towards reconciling experimental and computational determinations of Earth's core thermal conductivity. *Earth Planet. Sci. Lett.* **2022**, *584*, 117466. [CrossRef]
49. Secco, R.A. Thermal conductivity and Seebeck coefficient of Fe and Fe-Si alloys: Implications for variable Lorenz number. *Phys. Earth Planet. Inter.* **2017**, *265*, 23–34. [CrossRef]
50. Mao, H.-K.; Mao, W.L. *Treatise on Geophysics Volume 2 Mineral Physics*; Price, G.D., Schubert, G., Eds.; Elsevier Ltd.: Waltham, MA, USA, 2007; pp. 231–267.
51. Ryzhenko, B.; Kennedy, G.C. The Effect of Pressure on the Eutectic in the System Fe-FeS. *Am. J. Sci.* **1973**, *273*, 803–810. [CrossRef]
52. Buono, A.S.; Walker, D. H, not O or pressure, causes eutectic T depression in the Fe-FeS System to 8 Gpa. *Meteorit. Planet. Sci.* **2014**, *50*, 547–554. [CrossRef]
53. Weiss, R.J.; Marotta, A.S. Spin-dependence of the resistivity of magnetic metals. *J. Phys. Chem. Solids* **1959**, *9*, 302–308. [CrossRef]
54. Silber, R.E.; Secco, R.A.; Yong, W.; Littleton, J.A.H. Electrical resistivity of liquid Fe to 12 GPa: Implications for heat flow in cores of terrestrial bodies. *Sci. Rep.* **2018**, *8*, 10758–10759. [CrossRef]
55. Chen, B.; Gao, L.; Funakoshi, K.; Li, J. Thermal expansion of iron-rich alloys and implications for the Earth's core. *Proc. Natl. Acad. Sci. USA* **2007**, *104*, 9162–9167. [CrossRef]
56. Zhang, J.; Guyot, F. Thermal equation of state of iron and Fe 0.91 Si 0.09. *Phys. Chem. Miner.* **1999**, *26*, 206–211. [CrossRef]
57. Morard, G.; Bouchet, J.; Rivoldini, A.; Antonangeli, D.; Roberge, M.; Boulard, E.; Denoeud, A.; Mezouar, M. Liquid properties in the Fe-FeS system under moderate pressure: Tool box to model small planetary cores. *Am. Mineral.* **2018**, *103*, 1770–1779.
58. Pommier, A. Experimental investigation of the effect of nickel on the electrical resistivity of Fe-Ni and Fe-Ni-S alloys under pressure, *Am. Mineral.* **2020**, *105*, 1069–1077. [CrossRef]
59. Kuang, W.; Bloxham, J. An Earth-like numerical dynamo model. *Nature* **1997**, *389*, 371–374. [CrossRef]
60. Stevenson, D.J. Planetary Magnetic Fields: Achievements and Prospects. *Space Sci. Rev.* **2010**, *152*, 651–664. [CrossRef]
61. Sanloup, C.; Guyot, F.; Gillet, P.; Fiquet, G.; Mezouar, M.; Martinez, I. Density measurements of liquid Fe-S alloys at high pressure. *Geophys. Res. Lett.* **2000**, *27*, 811–814. [CrossRef]